Gradient-Based Coded-FM Waveform Design using Legendre Polynomials

Patrick M. McCormick and Shannon D. Blunt
Radar Systems Lab, University of Kansas, Lawrence, KS, USA

Keywords: FM waveform optimization, quasi-Newton method, Legendre polynomials

Abstract

A novel waveform optimization metric is proposed that encapsulates both the continuous-time nature of a frequency-modulated (FM) waveform and the discrete-time nature of the pulse compression receive filter. A continuous-time waveform model is used whose phase function is defined as a weighted sum of Legendre polynomials, thus parameterizing the continuous-time waveform with a discrete set of coefficients. Leveraging a novel correlation function that captures receiver range straddling effects, a q-norm integrated sidelobe metric is minimized using the gradient with respect to the discrete waveform parameters within a quasi-Newton formulation.

1 Introduction

A considerable portion of traditional FM waveform design relies on the principle of stationary phase (POSP) [1-4] where, given a prescribed amplitude envelope, the phase function of an FM waveform that approximates a desired spectral shape can be determined. This approximation becomes more accurate as the time-bandwidth product increases. By leveraging the power spectrum / autocorrelation Fourier pair, the power spectrum shape is thus chosen to correspond to an autocorrelation with low sidelobes.

It has recently been shown that polyphase codes, the parameterized structures of which permit the use of various optimization techniques, can be implemented as polyphase-coded FM (PCFM) waveforms [5] via a variant of continuous phase modulation from communications. Subsequently, [6] demonstrated that the continuous-time PCFM waveforms can be optimized using gradient-based methods since the waveform is defined using a discrete set of parameters.

In [6], a generalized integrated sidelobe (GISL) metric for FM waveforms was introduced that takes the q-norm ratio of the autocorrelation sidelobes to the autocorrelation mainlobe according to a specified receiver sampling rate. Here, the GISL metric is extended to include subsample shifts of the waveform inside the correlation function to minimize degradation of the pulse compression response due to range straddling effects [7].

Denoted generally as coded FM (CFM), the phase function model of the PCFM definition [5] is now expanded to include arbitrary weighted basis functions. Here, the particular case involving a weighted-sum of Legendre polynomials is examined. As an example, it is demonstrated that for waveforms of time-bandwidth less than 1024, only a small number of these polynomials (less than 12) are needed to produce a waveform with low autocorrelation sidelobes (with diminishing returns thereafter).

As further examples, two waveforms are optimized for experimental loopback testing using the CFM Legendre polynomial model: one with a rectangular amplitude envelope and the other with a Tukey envelope. The loopback correlation response agrees with the theoretical response in the rectangular case but deviates in Tukey case due to hardware distortion. The distortion was estimated and applied to the waveform model to produce a correlation response resembling that of the loopback test.

2 Coded FM waveform model

A complex-baseband FM waveform can be represented as

$$s(t) = u(t)\exp(j\phi(t)) , \qquad (1)$$

where $u(t)$ is the positive, real-valued, amplitude envelope and $\phi(t)$ is the continuous phase function. For pulsewidth T, define $s(t)$ over the interval $t \in [-0.5T, 0.5T]$. In general, the coded FM (CFM) phase function $\phi(t)$ can be represented as a weighted sum of N continuous-time basis functions as

$$\phi(t;\boldsymbol{\alpha}) = \sum_{n=1}^{N} \alpha_n \, g_n(t) , \qquad (2)$$

where $g_n(t)$ is the nth basis function and α_n is its corresponding real-valued weighting. For a given amplitude envelope $u(t)$ and set of basis functions $g_n(t)$, the FM waveform is completely parameterized by the N parameters $\boldsymbol{\alpha} = \begin{bmatrix}\alpha_1 & \alpha_2 & \cdots & \alpha_N\end{bmatrix}^T$. Note that this coded model subsumes PCFM [5] as one possible instantiation.

A natural basis for the phase function defined in (2) is a polynomial basis. Furthermore, it is advantageous to select functions that are orthogonal over a certain interval to avoid highly correlated basis functions. Thus we consider Legendre polynomial functions which are orthogonal over $x \in [-1, 1]$, where the vth polynomial is defined as [8]

$$P_v(x) = \frac{1}{2^v} \sum_{i=0}^{v} \binom{v}{i}^2 (x-1)^{v-i} (x+1)^i . \qquad (3)$$

For example, Fig. 1 depicts the Legendre polynomial functions for $v \in \{1,4,7,12\}$. Since the Legendre polynomial functions are orthogonal over $x \in [-1, 1]$, each parameter α_n corresponds to a unique basis function $g_n(t)$.

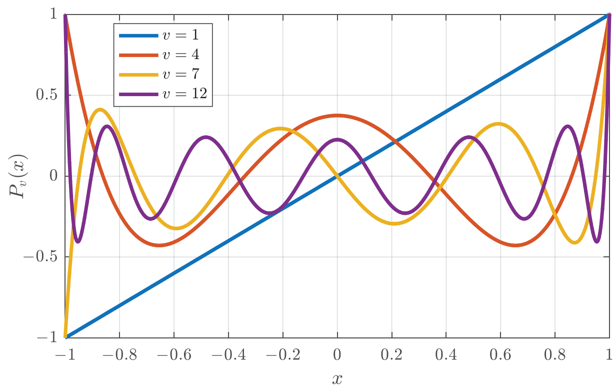

Fig. 1: Legendre polynomial functions $P_v(x)$ for $v \in \{1,4,7,12\}$

Note that even values of v produce even (symmetric) functions, while odd values produce odd (antisymmetric) functions. Thus we shall limit attention to the even symmetric functions $v \in \{2,4,6...\}$ as they yield symmetric frequency responses (given that $u(t)$ is also symmetric). Therefore the CFM basis functions are set as

$$g_n(t) = P_{2n}(2t/T) \quad \text{for} \quad n = 1, \cdots, N. \tag{4}$$

3 Continuous correlation using a digital filter

The ambiguity function is a standard tool with which to evaluate the "goodness" of a radar waveform. For the waveform model in (1), the ambiguity function is defined as

$$\chi(\tau, f_d) = \frac{1}{T} \int_{-T/2}^{T/2} s^*(t-\tau)\ s(t) \exp\left(j2\pi f_d t\right) dt \tag{5}$$

for delay τ and Doppler frequency f_d. The zero Doppler slice of the delay/Doppler ambiguity function (i.e. the continuous-time waveform autocorrelation) is

$$\chi(\tau, f_d = 0) = \frac{1}{T} \int_{-T/2}^{T/2} s^*(t-\tau)\ s(t)\ dt, \tag{6}$$

which is the ideal matched filter response for waveform $s(t)$. However, the expression in (6) does not capture the interaction of the continuous-time waveform that is physically emitted by the transmitter with the digital (and thus discrete-time) pulse compression filter on receive, though the ideal response can be well approximated if the receiver sampling rate is much higher than the waveform 3-dB bandwidth [5,9]. With rapid advances in diverse waveform design and generation [10], this interaction is becoming increasingly more common.

To address this limitation, we propose the alternative correlation function

$$A(\tau) = \frac{1}{M} \int_{-T/2}^{T/2} \tilde{s}^*(t-\tau;\xi)\ s(t)\ dt, \tag{7}$$

where

$$\tilde{s}(t;\xi) = \sum_{m=0}^{M-1} s(mT_s + \xi)\ \delta(t - mT_s - \xi) \tag{8}$$

is a train of M weighted impulses at time instants $mT_s + \xi$ for $m \in \{0, \ldots, M-1\}$. The term $T_s = 1/f_s = T/M$ is the receiver sampling period and $\xi \in (0, T_s)$ is a sub-sample delay offset. The impulse train weights, which are discretized samples of waveform $s(t)$, correspond to the length-M discrete matched filter $\tilde{\mathbf{s}}(\xi) = [s(\xi)\ \ s(T_s+\xi)\ \ \cdots\ \ s((M-1)T_s+\xi)]^T$ for delay offset ξ and sampling period T_s.

The receiver sampling rate f_s is K times (over-sampled) the 3-dB bandwidth B to provide sufficient fidelity of the FM waveform. Therefore, the length of the discrete matched filter is $M = KBT$, which corresponds to the available waveform design degrees of freedom [6]. Here we shall use an over-sampling factor of $K = 2$ which is practically achievable for many radar applications.

Correlating the waveform $s(t)$ with the weighted impulse train $\tilde{s}(t;\xi)$ naturally accounts for the continuous nature of the physical radar emissions and the subsequent digital filtering in the radar receiver. The particular delay values $\tau = \ell T_s$ for discrete index $-M+1 \le \ell \le M-1$ of the correlation function $A(\tau)$ represent the discrete-time autocorrelation of $\tilde{\mathbf{s}}(\xi)$ as

$$A(\ell T_s) = \frac{1}{M} \sum_{m=0}^{M-1} s^*\left((m-\ell)T_s + \xi\right) s\left(mT_s + \xi\right). \tag{9}$$

All other delays in $-T \le \tau \le T$ correspond to range straddling conditions that can elicit mismatch loss [7] and possibly sidelobe degradation [5,9]. By defining the waveform/filter correlation using (7) so that these range straddling effects are included, subsequent evaluation of the range sidelobes via metrics such as peak sidelobe level (PSL) or integrated sidelobe level (ISL) inherently address the finite degrees of freedom of the receive filter.

4 Optimization Procedure for CFM waveforms

In [6], a q-norm optimization metric for FM waveforms called the Generalized Integrated Sidelobe Level (GISL) was introduced and defined as

$$J_q(\boldsymbol{\alpha}) = \left(\frac{\int_{\Delta\tau}^{T} |A(\tau)|^q \, d\tau + \int_{-T}^{-\Delta\tau} |A(\tau)|^q \, d\tau}{\int_{-\Delta\tau}^{\Delta\tau} |A(\tau)|^q \, d\tau} \right)^{1/q} \tag{10}$$

for $q \geq 2$. Note that $q = 2$ is the Integrated Sidelobe Level (ISL) and $q \to \infty$ yields the Peak Sidelobe Level (PSL). Values of q between these cases strike a balance between the ISL and PSL metrics. A similar metric to (10) has also recently been proposed for the design of phase codes [11,12]. Here, the modified correlation function defined in (7) is included in (10) to incorporate sub-sample shifts in the waveform.

The variability of the cost function in (10) with norm q can drastically change the autocorrelation properties of a resulting (iteratively) optimized waveform given the same waveform initialization. For the case of a rectangular-envelope $u(t)$, a $q = 5$ norm has been found to retain both ISL and PSL properties.

The term $\Delta\tau$ in (10) defines the peak-to-null mainlobe width and is related to 3-dB bandwidth as $\Delta\tau \approx 1/B$. Thus the time-bandwidth product is $BT \approx T/\Delta\tau$. Therefore, the time-bandwidth for waveform optimization can effectively be set by establishing the relative peak-to-null mainlobe width $T/\Delta\tau$ without explicit shaping of the waveform spectrum.

Observe that, for $2 \leq q < \infty$, the metric in (10) is a continuous function of the length-N parameter vector $\boldsymbol{\alpha}$ through the combination of (1), (2), and (7). As such, gradient-based optimization methods (e.g. nonlinear conjugate gradient [6], quasi-Newton method, etc.) can be implemented to minimize this metric [13]. Of course, it should be noted that the gradient of $J_{q\to\infty}(\boldsymbol{\alpha})$ is discontinuous, and thus gradient-based PSL optimization can only be approximated for q large.

Here, a quasi-Newton gradient-descent method with a Broyden-Fletcher-Goldfarb-Shanno Hessian approximation update is used to minimize (10), with the gradient calculated using a finite-difference approximation [13]. As for all gradient-based methods, the algorithm descends onto a locally optimal solution which is not guaranteed to be globally optimal. Therefore the locally optimal solution is highly dependent on the initialization. As such, an order-recursive approach is implemented to ensure the quasi-Newton method is initialized with a waveform that already has good autocorrelation properties.

Given the N basis functions from (4), the order-recursive approach is initiated by first performing the quasi-Newton search only using the lowest order basis function $g_1(t)$, which corresponds to an order-2 polynomial. The converged waveform after gradient-descent optimization is then used as an initialization for the order-4 polynomial that uses basis functions $g_1(t)$ and $g_2(t)$, for the quasi-Newton search is likewise performed. For a predefined N, this order-recursive process is repeated until all basis functions $g_n(t)$, for $n = 1, \ldots, N$, have been incorporated into the optimization.

5 Simulations and Loopback Measurements

It is first useful to determine the optimal offset delay ξ for the receive filter and the sufficient number of basis functions N as a function of BT. Using this knowledge, two waveforms are then optimized: one with a rectangular amplitude envelope and one with a 10% Tukey tapered envelope. These waveforms are evaluated on hardware in a loopback configuration and their filter responses are compared to the theoretical autocorrelation responses.

5.1 Sample offset and number of basis functions

The quasi-Newton gradient-descent optimization procedure was implemented to determine the optimal sample offset ξ, for $\tilde{s}(t;\xi)$ the digital receive filter. The normalized offset parameter is varied from $\xi/T_s = 0$ to $\xi/T_s = 1$, with the remaining parameters set to $BT = 128$, $K = 2$, $N = 32$ basis functions, a rectangular amplitude envelope $u(t)$, and $q = 5$.

Figure 2 shows the converged values of $J_5(\boldsymbol{\alpha}_{\min})$ versus normalized sample delay ξ/T_s, where we find that $\xi/T_s = 0.5$ provides the minimum value. Unsurprisingly, this condition arises because delay $\xi/T_s = 0.5$ is equidistant (in time) from the extremes of range-straddling that may occur. The subsample offset of $\xi/T_s = 0.5$ is used for the remainder of the paper.

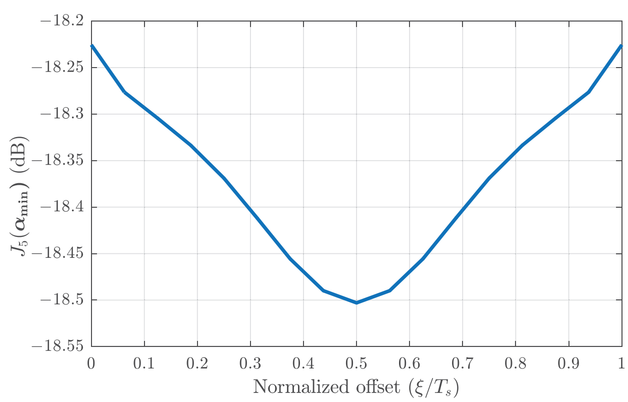

Fig. 2: Values of $J_5(\boldsymbol{\alpha}_{\min})$ versus normalized offset ξ / T_s

To determine a sufficient number of basis functions to characterize the phase function $\phi(t)$, Fig. 3 plots the cost function $J_5(\boldsymbol{\alpha}_{\min})$ from (10) as a function of N for the values $BT \in \{64, 128, 256, 512, 1024\}$. As before, $K = 2$ and $u(t)$ has a rectangular envelope. It is observed that for each BT there are two regimes: one in which $J_5(\boldsymbol{\alpha}_{\min})$ decreases rapidly with increasing N and then a 'diminishing return' region where $J_5(\boldsymbol{\alpha}_{\min})$ decreases much more slowly with increasing N. The transition between these regions depends on BT but is found to be between $N=6$ and $N=12$ for the cases considered. For the remainder of the paper we shall use $N=32$ basis functions which resides well within the second region.

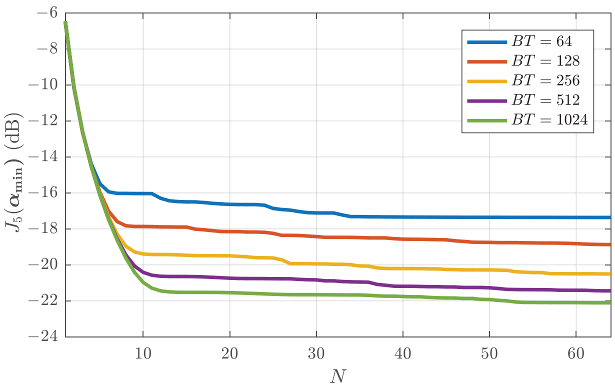

Fig. 3: Values of $J_5(\boldsymbol{\alpha}_{\min})$ versus N for different BT

5.2 Optimized CFM waveforms

Two waveforms of $BT=200$ are optimized for an over-sampling of $K=2$ using $N=32$ Legendre polynomials as basis functions (polynomial order of 64). The first waveform has a rectangular amplitude envelope (labelled RECT) and its optimization uses q = 5 in (10). The second waveform has a 10% Tukey tapered envelope (labelled TUKEY) and its optimization uses q = 2 in (10), which has been found to produce a lower overall sidelobe level than q = 5 for this amplitude envelope.

Figure 4 shows the power spectra of the RECT-envelope (blue) and TUKEY-envelope (red) waveforms with the receiver sampled bandwidth ($f_s = KB = 2B$) indicated by the vertical dashed lines. Note that by setting the relative peak-to-null width $T/\Delta\tau$ in the optimization, we have effectively established the desired 3-dB bandwidth of the RECT and TUKEY-envelope waveforms. While the in-band spectral content of the two waveforms is nearly identical, the TUKEY-envelope case has a much sharper roll-off. This result is not unexpected since the abrupt on/off transition of the rectangular envelope will exhibit a sin(x)/x spectral skirt. For comparison, a rectangular-windowed linear FM (LFM-R) and Tukey-windowed linear FM (LFM-T) with similar time-bandwidth products are included. While all the waveforms have similar 3-dB power bandwidths, the optimized waveform spectra clearly exhibit some spectral broadening.

While the optimization via (10) uses the hybrid continuous/discrete autocorrelation of (7) to account for straddling effects, it is easier to depict the final result using the discrete autocorrelation of (9). The autocorrelation responses (using (9)) are shown in Fig. 5 for the RECT-envelope optimized waveform (blue) and the rectangular-windowed LFM (red). The maximum straddled responses from (7) are also shown in dark blue and dark red, respectively, which represent the worst-case responses for these waveforms. The maximum PSL of the optimized waveform is –44.75 dB, as compared to –13.36 dB for the LFM-R case.

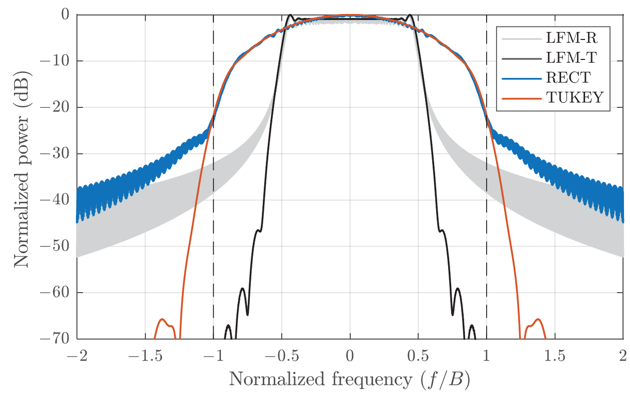

Fig. 4: Power spectra of LFM-R (gray), LFM-T (black), optimized RECT-envelope waveform (blue), and optimized TUKEY-envelope waveform (red). Receiver sampled bandwidth indicated by vertical dashed lines.

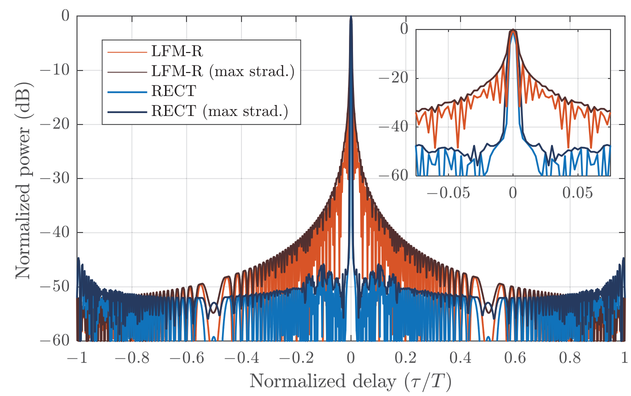

Fig. 5: Autocorrelation via (9) for LFM-R (red) and optimized RECT-envelope waveform (blue). Maximum straddled responses in dark blue and dark red, respectively.

Figure 6 shows the autocorrelation responses (using (9)) for the TUKEY-envelope optimized waveform (blue) and the Tukey-windowed LFM (red). The maximum straddled responses from (7) are likewise shown in dark blue and dark red, respectively. The Tukey-tapered waveform achieves much lower sidelobes compared to the RECT-envelope optimized waveform from Figure 5 while only incurring 0.56 dB in SNR loss due to the tapering. As compared to the LFM-T response, the energy close to the mainlobe is reduced for the TUKEY-envelope optimized waveform, though sidelobes of approximately –57 dB are observed at the autocorrelation edges. These further-out sidelobes can be readily mitigated through the use of appropriate optimal mismatch filtering on receive with minimal additional loss (see [9]).

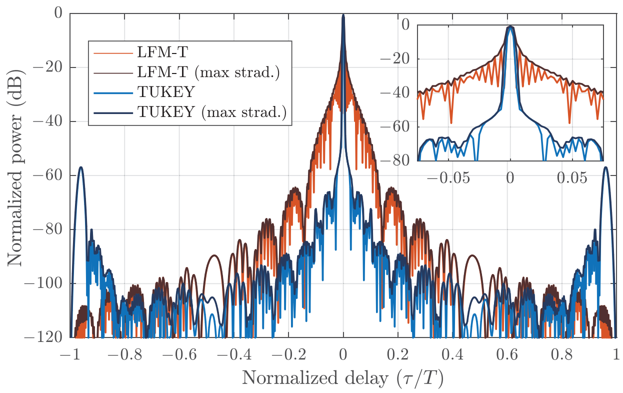

Fig. 6: Autocorrelation via (9) for LFM-T (red) and optimized TUKEY-envelope waveform (blue). Maximum straddled responses in dark blue and dark red, respectively.

Figures 7 and 8 depict the ambiguity functions (via (5)) for both the RECT-envelope and TUKEY-envelope optimized waveforms, respectively. Both waveforms exhibit a delay-Doppler ridge similar to that of an LFM waveform indicating these waveforms are relatively Doppler tolerant.

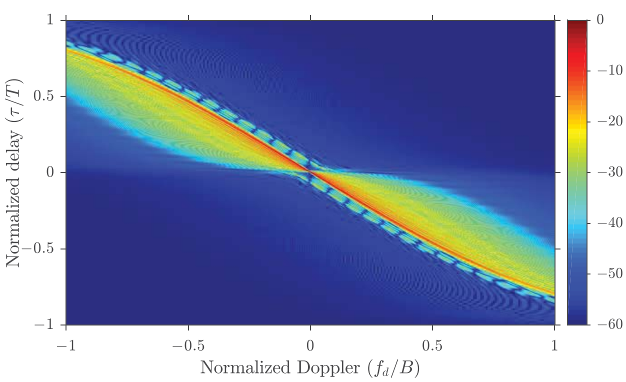

Fig. 7: Ambiguity function $|\chi(\tau, f_d)|$ (in dB) via (5) of the RECT-envelope optimized waveform.

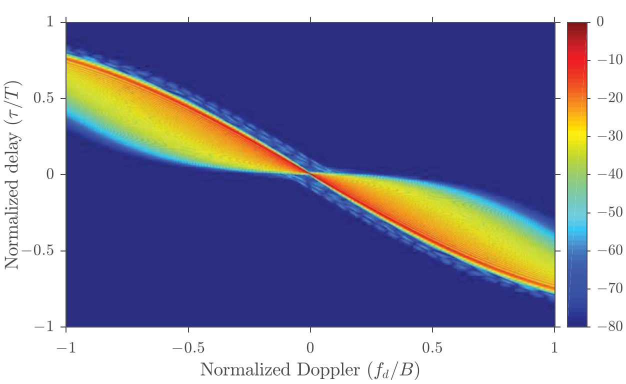

Fig. 8: Ambiguity function $|\chi(\tau, f_d)|$ (in dB) via (5) of the TUKEY-envelope optimized waveform.

5.3 Hardware loopback measurements

The two optimized waveforms were tested in a loopback configuration using a Tektronix AWG70002A arbitrary waveform generator (10-bit) and a Rohde & Schwarz FSW 26 real-time spectrum analyzer (18-bit) to evaluate the degradation of the waveforms when filtered, down-sampled, and represented with finite bit-depth. The bandwidth of the waveforms was set at $B = 50$ MHz with a pulse duration of $T = 4\ \mu s$. For $K = 2$ over-sampling the receiver sampling rate was set to $f_s = 100$ MHz.

Figure 9 shows the loopback response (red) and the theoretical autocorrelation via (9) (blue) for the RECT-envelope optimized waveform. The loopback measurement results in 0.01 dB in mismatch loss due to either straddling or filtering, while the sidelobe responses are almost identical. Figure 10 likewise shows the loopback and theoretical autocorrelation responses for the Tukey-tapered optimized waveform. A mismatch loss of only 0.01 dB is once again observed. However, the sidelobe response of the loopback data is noticeably different from the lower sidelobes of theoretical response.

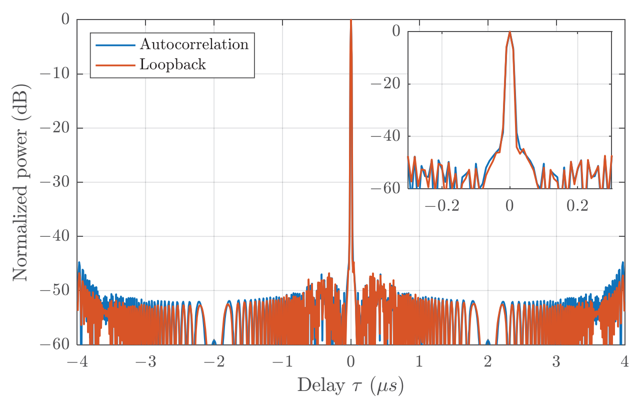

Fig. 9: Theoretical autocorrelation (blue) via (9) and hardware loopback correlation (red) for the RECT-envelope optimized waveform.

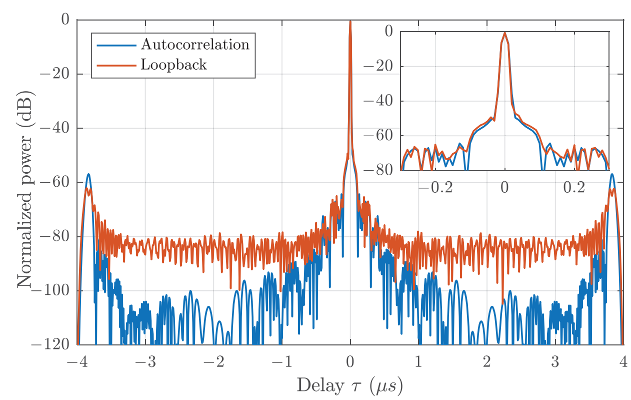

Fig. 10: Theoretical autocorrelation (blue) via (9) and hardware loopback correlation (red) for the TUKEY-envelope optimized waveform.

The distortion of the waveform due to up-conversion, down-conversion, linear filtering, and finite bit-depths of the loopback setup was estimated and applied to the continuous-time waveform model in (1) for the TUKEY-envelope optimized waveform. Figure 11 shows the correlation response of the loopback test and the estimated response when incorporating the knowledge of these practical effects. The responses now resemble one another much more closely than was observed in Figure 10. In the same manner as the ultra-low sidelobes achieved in [14], this result indicates that more knowledge of the distortion imposed by the RF transmit/receive chain needs to be incorporated into the waveform model to realize the fidelity necessary to achieve the promised performance gains of advanced waveform design and, by extension, waveform diversity [10].

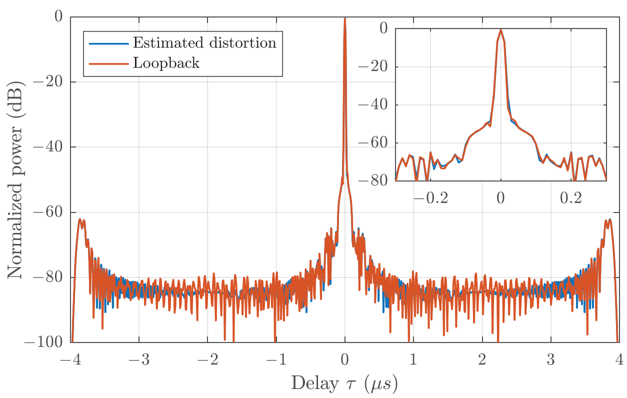

Fig. 11: Correlation response with estimated loopback distortion (blue) and hardware loopback correlation (red) for the TUKEY-envelope optimized waveform.

5 Conclusion

The design of Legendre-polynomial coded waveforms was demonstrated using quasi-Newton method optimization. A correlation function was also defined that allows this optimization to account for range straddling effects. It was found that the orthogonal nature of Legendre polynomials facilitates the design of waveforms with quite low sidelobe levels with a very small number of code values. Experimental loopback measurements demonstrated the efficacy of this design procedure for both rectangular-envelope and Tukey-envelope optimized waveforms. Below –80 dB it was observed that the distortion of the RF test equipment had to be taken into account to represent the waveform with sufficient fidelity.

Acknowledgements

This work was supported by a subcontract with Matrix Research, Inc. for research sponsored by AFRL under Prime Contract #FA8650-14-D-1722.

References

[1] C.E. Cook, “A class of nonlinear FM pulse compression signals,” *Proc. IEEE*, vol. 52, no. 11, pp. 1369-1371, Nov. 1964.

[2] E. Fowle, “The design of FM pulse compression signals,” *IEEE Trans. Information Theory*, vol. 10, no. 1, pp. 61-67, Jan. 1964.

[3] J.A. Johnston, A.C. Fairhead, “Waveform design and Doppler sensitivity analysis for nonlinear FM chirp pulses,” *IEE Proc. Communications, Radar & Signal Processing*, vol. 133, no. 2, pp. 163-175, Apr. 1986.

[4] N. Levanon, E. Mozeson. *Radar Signals*, Wiley-IEEE Press, 2004.

[5] S.D. Blunt, M. Cook, J. Jakabosky, J.D. Graaf, E. Perrins, "Polyphase-coded FM (PCFM) radar waveforms, part I: implementation," *IEEE Trans. Aerospace and Electronic Systems*, vol. 50, no. 3, pp. 2218-2229, July 2014.

[6] P.M. McCormick, S.D. Blunt, “Nonlinear conjugate gradient optimization of polyphase-coded FM radar waveforms,” *IEEE Radar Conf.*, Seattle, WA, USA, May 2017.

[7] M.A. Richards, J.A. Scheer, W.A. Holm. *Principles of Modern Radar: Basic Principles*. SciTech, 2010, pp. 786-787.

[8] M. Abramowitz and I.A. Stegun. *Handbook of Mathematical Functions*, vol. 55. Courier Corporation, 1964, chap. 8.

[9] D. Henke, P. McCormick, S.D. Blunt, T. Higgins, "Practical aspects of optimal mismatch filtering and adaptive pulse compression for FM waveforms," *IEEE Radar Conf.*, Washington, DC, USA, May 2015.

[10] S.D. Blunt, E.L. Mokole, "An overview of radar waveform diversity," *IEEE Aerospace and Electronic Systems Mag.*, vol. 31, no. 11, pp. 2-42, Nov. 2016.

[11] B. O'Donnell, J.M. Baden, "Fast gradient descent for multi-objective waveform design," *IEEE Radar Conf.*, Philadelphia, PA, USA, May 2016.

[12] J. Song, P. Babu, D.P. Palomar, "Sequence design to minimize the weighted integrated and peak sidelobe levels," *IEEE Trans. Signal Processing*, vol. 64, no. 8, pp. 2051-2064, Apr. 2016.

[13] J. Nocedal, S. Wright. *Numerical Optimization*, Springer Science & Business Media, 2006.

[14] J. Jakabosky, S.D. Blunt, T. Higgins. "Ultra-low sidelobe waveform design via spectral shaping and LINC transmit architecture," *IEEE Intl. Radar Conf.*, Washington, DC, USA, May 2015.